J. Fluid Mech. (1981), *vol.* 112, *pp.* 329–345
Printed in Great Britain

Magnetohydrodynamic Taylor vortex flows

By P. TABELING

Laboratoire de Génie Electrique de Paris associé au C.N.R.S.,
E.S.E. Plateau du Moulon 91190, Gif-sur-Yvette

(Received 30 September 1980 and in revised form 19 May 1981)

Hydromagnetic Taylor-vortex flows of liquid metals, subjected to an axially applied magnetic field, are considered. The supercritical state of flow is treated by means of perturbation method with multiple scale expansions in time and space. Results show that the supercritical state of flow is significantly affected by the imposed magnetic field. Calculations on finite equilibrium amplitude of Taylor vortices are compared with experiment. In the case of Taylor–Couette flows between insulating cylinders, good agreement is found between theory and experiment, while, in the case of electromagnetically driven flows between steady conducting cylinders, disagreement occurs once magnetic field effects become significant. These results are discussed.

1. Introduction

Hydromagnetic Taylor vortex flows of liquid metals have been extensively studied. However, most papers are concerned only with the first bifurcation of such flows. It is known from Chandrasekhar (1961) and Chang & Sartory (1967) that the first instability in liquid metal flows between infinite concentric cylinders, subjected to an axially applied magnetic field, is dramatically affected by the conductivities of the cylinders. When cylinders are insulating, Taylor cells elongate in the direction of magnetic field lines (as shown by Chandrasekhar) while, in the other case (conducting cylinders), Taylor cells generally contract in the axial direction (Chang & Sartory 1967). Also of importance is the stabilizing effect of the applied magnetic field, which is found to be much stronger in the conducting than in the insulating case. So far, hydromagnetic Taylor-vortex flows exhibit profoundly distinct features depending on the conductivity of the cylinders.

Above transition, hydrodynamic stability theory predicts that Taylor vortices grow exponentially with time and attain a finite equilibrium amplitude once nonlinear effects become significant. In the case of magnetohydrodynamic flows of liquid metals, similar processes occur; however, constants of the flow above transition are profoundly affected by the magnetic field. In an earlier work, Moffatt (1962) calculated the expression of those constants in the case of Taylor vortex flows between rotating cylinders in the presence of a toroidal magnetic field. Flows considered herein are subjected to an axially applied magnetic field; they are driven either by the rotation of the inner cylinder, the outer one being at rest, or by a constant transverse pressure gradient.

The mathematical method involved in the present paper is based on a perturbation scheme in terms of a small parameter ϵ with multiple scale expansions in time and space;

to first order, ϵ reduces to the discrepancy $[(T/T_c)^{\frac{1}{2}}-1]^{\frac{1}{2}}$ in which T is the Taylor number and T_c is the critical value of T. Further theoretical results are compared with experiments, in which measures are obtained, either on the torque required to maintain the flow (Donnelly & Ozima 1962 in the Taylor–Couette case), or on the mean spatial azimuthal motion (Baylis 1962; Tabeling & Chabrerie 1981*a* for electromagnetically driven flows).

2. Equations of flow

Consider isothermal liquid metal flows between infinite concentric cylinders, as shown in figure 1. The radii of the cylinders are R_1, R_2 (with $R_1 < R_2$), and the gap $d = R_2 - R_1$ is supposed to be much smaller than R_1. The flow is subjected to a constant uniform magnetic field B_0 directed axially and the fluid is driven either by the rotation of the inner cylinder at constant angular speed Ω_1, or by a constant transverse body force K. The latter is formally written as $K = R_1^{-1}(\partial P/\partial\theta)$, where P is the pressure and θ is the angular co-ordinate. Two cases are considered: (I) all cylinders insulating and (C) all cylinders perfectly conducting. We suppose that the flow is axisymmetric, so that all derivatives $\partial/\partial\theta$ are set equal to zero, except that for the pressure P.

Equations of flow under the assumptions of small magnetic Reynolds numbers $R_m = \sigma\mu_0 U^* d$ (where σ, μ_0, U^* are respectively the fluid conductivity, the vacuum permittivity and a characteristic velocity scale), and small magnetic Prandtl number $P_m = \sigma\mu_0\nu$ (where ν is the kinematic viscosity) have been established in previous papers (see Tabeling & Chabrerie 1981*a*, *b*, or others); we have

$$\frac{\partial U_R}{\partial t} + U_R\frac{\partial U_R}{\partial X} + U_Z\frac{\partial U_R}{\partial Z} - \frac{U_\theta^2}{R_1} = -\frac{1}{\rho}\frac{\partial P}{\partial X} - \frac{\sigma B_0^2}{\rho}U_R + \nu\,\Delta U_R, \tag{1}$$

$$\frac{\partial U_\theta}{\partial t} + U_R\frac{\partial U_\theta}{\partial X} + U_Z\frac{\partial U_\theta}{\partial Z} = \frac{K}{\rho} + \frac{B_0}{\rho}\frac{\partial H_\theta}{\partial Z} + \nu\,\Delta U_\theta, \tag{2}$$

$$\frac{\partial U_Z}{\partial t} + U_R\frac{\partial U_Z}{\partial X} + U_Z\frac{\partial U_Z}{\partial Z} = -\frac{1}{\rho}\frac{\partial P}{\partial Z} + \nu\,\Delta U_Z, \tag{3}$$

$$\Delta H_\theta + \sigma B_0\frac{\partial U_\theta}{\partial Z} = 0, \tag{4}$$

and

$$\frac{\partial U_R}{\partial X} + \frac{\partial U_Z}{\partial Z} = 0, \tag{5}$$

with

$$\Delta = \partial^2/\partial X^2 + \partial^2/\partial Z^2.$$

In (1)–(5), U_R, U_θ and U_Z are the velocity components, P is the pressure, and H_θ is the azimuthal component of the induced magnetic field; t is the time, Z is the distance along the cylinders' axis, and $X = R - R_1$ (where R is the radial co-ordinate); ρ is the density of the fluid.

The boundary conditions are:

$$U_R = U_Z = 0, \quad U_\theta = \Omega_1 R_1, \quad H_\theta = 0 \text{ (case I)} \quad \text{or} \quad \partial H_\theta/\partial X = 0 \text{ (case C)} \quad \text{on} \quad X = 0 \quad \text{and} \quad X = d. \tag{6}$$

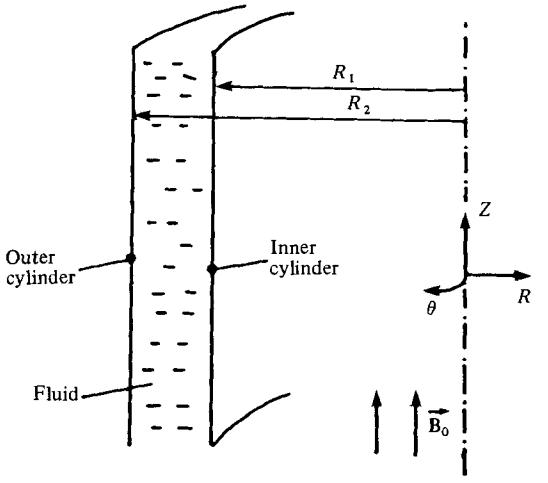

FIGURE 1. Schematic diagram of the flow.

Equations (1)–(5) admit an exact solution $U_\theta^{(0)}$, $H_\theta^{(0)}$, $P^{(0)}$ calculated to be

$$U_\theta^{(0)} = \frac{K}{2\rho\nu} X(X-d) + \Omega_1 R_1 (1 - X/d), \quad P^{(0)} = K\theta R_1 + \frac{\rho}{R_1}\int_0^d U_\theta^{(0)2}\, dX \quad \text{and} \quad H_\theta^{(0)} = 0. \tag{7}$$

(7) defines the laminar primary flow.

The governing equations for axisymmetric perturbations to the primary flow as defined in (7) are found to be (in dimensionless form)

$$\frac{\partial u_r}{\partial \tau} + u_r \frac{\partial u_r}{\partial x} + u_z \frac{\partial u_r}{\partial z} = -\frac{\partial p}{\partial x} - Q u_r + \Delta u_r + T^{\frac{1}{2}} u_\theta^{(0)} u_\theta + \tfrac{1}{2} u_\theta^2, \tag{8}$$

$$\frac{\partial u_\theta}{\partial \tau} + u_r \frac{\partial u_\theta}{\partial x} + u_z \frac{\partial u_\theta}{\partial z} = Q \frac{\partial h_\theta}{\partial z} + \Delta u_\theta - T^{\frac{1}{2}} u_r \frac{du_\theta^{(0)}}{\partial x}, \tag{9}$$

$$\frac{\partial u_z}{\partial \tau} + u_r \frac{\partial u_z}{\partial x} + u_z \frac{\partial u_z}{\partial z} = -\frac{\partial p}{\partial z} + \Delta u_z, \tag{10}$$

$$\Delta h_\theta + \frac{\partial u_\theta}{\partial z} = 0, \tag{11}$$

and

$$\frac{\partial u_r}{\partial x} + \frac{\partial u_z}{\partial z} = 0, \tag{12}$$

where now $\Delta = \partial^2/\partial x^2 + \partial^2/\partial z^2$, and

$$\left.\begin{aligned} &u_r = U_r \frac{d}{\nu}, \quad u_\theta = (U_\theta - U_\theta^{(0)})\, d(2\sigma)^{\frac{1}{2}}/\nu, \quad u_z = U_z d/\nu, \\ &h_\theta = H_\theta (2\delta)^{\frac{1}{2}}/\sigma\nu B_0, \quad x = X/d, \quad z = Z/d, \quad \tau = \nu t/d^2, \\ &u_\theta^{(0)} = U_\theta^{(0)}/U_e, \quad T = 2U_e^2 d^2/\nu^2 \quad \text{(Taylor number)}, \\ &Q = \sigma B_0^2 d^2/\rho\nu \quad \text{(Chandrasekhar number)} \quad \text{and} \quad \delta = \frac{d}{R_1} \quad \text{(curvature ratio)}, \end{aligned}\right\} \tag{13}$$

where U_e is a velocity scale which we shall define later. The boundary conditions are

$$u_r = u_\theta = u_z = 0, \quad h_\theta = 0 \text{ (case I)} \quad \text{or} \quad \frac{\partial h_\theta}{\partial x} = 0 \text{ (case C)} \quad \text{on} \quad x = 0 \quad \text{and} \quad x = 1. \tag{14}$$

3. Linear stability analysis

We consider infinitesimal perturbations of the form:

$$u_r = u(x)\,e^{\Lambda\tau+iaz}, \quad u_\theta = v(x)\,e^{\Lambda\tau+iaz}, \quad u_z = -iw(x)\,e^{\Lambda\tau+iaz},$$
$$p = \pi(x)\,e^{\Lambda\tau+iaz} \quad \text{and} \quad h_\theta = -ih(x)\,e^{\Lambda\tau+iaz}, \tag{15}$$

in which Λ is the linear growth rate of disturbances and a is the convective wavenumber. The linearized form of perturbation equations (8)–(12) reduces to

$$[(D^2-a^2)^2-\Lambda(D^2-a^2)+Qa^2]\,u = T^{\frac{1}{2}}au_\theta^{(0)}(D^2-a^2)\,h,$$
$$[(D^2-a^2)^2-\Lambda(D^2-a^2)+Qa^2]\,h = T^{\frac{1}{2}}aDu_\theta^{(0)}u, \tag{16}$$

together with

$$u = Du = (D^2-a^2)\,h = 0, \quad h = 0 \text{ (case I)} \quad \text{or} \quad Dh = 0 \text{ (case C)} \quad \text{on} \quad x = 0 \quad \text{and} \quad x = 1, \tag{17}$$

where $D = d/dx$.

The eigenvalue system of equations (16) defines the linear growth rate Λ as a function of Q, a and T, i.e. $\Lambda = \Lambda(Q, a, T)$. Assuming that the principle of exchange of stability holds and the marginal state is stationary, we set $\Lambda = 0$ in (16) and obtain the governing equations for the marginal state in the form

$$\mathscr{A}\phi_j = T_j^{\frac{1}{2}}\mathscr{B}\phi_j, \tag{18}$$

with

$$\mathscr{A} = \begin{pmatrix} (D^2-a^2)+Qa^2 & 0 \\ 0 & (D^2-a^2)^2+Qa^2 \end{pmatrix},$$

and

$$\mathscr{B} = \begin{pmatrix} 0 & au_\theta^{(0)}(D^2-a^2) \\ aDu_\theta^{(0)} & 0 \end{pmatrix}. \tag{19}$$

In (18), $\phi_j = \begin{pmatrix} u_j \\ h_j \end{pmatrix}$ and T_j denote respectively the jth eigenvector and eigenvalue. The adjoint problem of (18) is $\mathscr{A}\tilde{\phi}_j = T_j\tilde{\mathscr{B}}\tilde{\phi}_j$, in which $\tilde{\phi}_j$ is the adjoint eigenvector while $\tilde{\mathscr{B}}$ is calculated to be:

$$\tilde{\mathscr{B}} = \begin{pmatrix} 0 & au_\theta^{(0)}D \\ a(D^2-a^2)\,[u_\theta^{(0)}] & 0 \end{pmatrix}. \tag{21}$$

The eigenvectors ϕ_j and $\tilde{\phi}_k$ satisfy the orthogonality relations in the form

$$(\tilde{\phi}_k|\,\mathscr{B}\,|\phi_j) = \int_0^1 \tilde{\phi}_k\mathscr{B}(\phi_j)\,dx \propto \delta_{jk}. \tag{22}$$

The eigenvalues of (18) constitute an infinite denumerable sequence of real numbers which can be ordered such that, for given Q and a,

$$T_{j+1} \geqslant T_j \quad \text{for} \quad j \geqslant 1.$$

It follows that the critical Taylor number T_c and critical wavenumber a_c satisfy the relation $\partial T_1/\partial a = 0$ for $T_1 = T_c$ and $a = a_c$. The latter condition can be rewritten in the form $(\tilde{\phi}_1|\,\mathscr{D}_1\,|\phi_1) = 0$ (see (18) and (22)), where $\mathscr{D}_1$ is defined as

$$\mathscr{D}_1 = \begin{pmatrix} -4a(D^2-a^2)+2Qa & -T_1^{\frac{1}{2}}au_\theta^{(0)} \\ -T_1^{\frac{1}{2}}Du_\theta^{(0)} & -4a(D^2-a^2)+2Qa \end{pmatrix}.$$

When T slightly exceeds T_c, the linear growth rate can be expanded in the form

$$\Lambda(Q, a, T) = c_0(Q)\,[(T/T_c)^{\frac{1}{2}} - 1] - c_1(Q)\,(a - a_c)^2, \tag{23}$$

where

$$c_0 = (\tilde{\phi}_1|\,\mathscr{B}\,|\phi_1)/(\tilde{\phi}_1|\,\mathscr{K}\,|\phi_1), \tag{24}$$

and

$$c_1 = (c_0/T_c)\,(\partial^2 T/\partial a^2)_{a=a_c}, \tag{25}$$

with

$$\mathscr{K} = \begin{pmatrix} D^2 - a^2 & 0 \\ 0 & D^2 - a^2 \end{pmatrix}. \tag{26}$$

It follows that Λ and $(a - a_c)$ are respectively $O(\epsilon^2)$ and $O(\epsilon)$ if $T^{\frac{1}{2}}/T_c^{\frac{1}{2}} - 1 = O(\epsilon^2)$ near the onset of instability.

4. Nonlinear analysis near criticality

The nonlinear state of flow near transition can be investigated by a perturbation method in terms of a small parameter ϵ. Expanding $\mathbf{u}(u_r, u_\theta, u_z)$, p, h_θ and T as series in ascending powers of ϵ, we find

$$\mathbf{u} = \epsilon\mathbf{u}^{(1)} + \epsilon^2\mathbf{u}^{(2)} + \epsilon^3\mathbf{u}^{(3)} + \ldots, \tag{27}$$

$$p = \epsilon p^{(1)} + \epsilon^2 p^{(2)} + \epsilon^3 p^{(3)} + \ldots, \tag{28}$$

$$h_\theta = \epsilon h^{(1)} + \epsilon^2 h^{(2)} + \epsilon^3 h^{(3)} + \ldots \tag{29}$$

and

$$T^{\frac{1}{2}} = T_c^{\frac{1}{2}} + \epsilon^2 T^{(2)} + \epsilon^3 T^{(3)} + \ldots. \tag{30}$$

Owing to (30) we can arbitrarily set $T^{(2)} = T_c^{\frac{1}{2}}$ without loss of generality. In view of the asymptotic behaviours of Λ and a near transition (see (23)) we consider a slowly varying process with characteristic time and length scales $O(\epsilon^{-2})$ and $O(\epsilon^{-1})$ respectively, and hence introduce the following variables:

$$\left.\begin{aligned} &\tau_0 = \tau, \quad \tau_2 = \epsilon^2\tau, \quad \tau_4 = \epsilon^4\tau, \quad \text{etc.} \\ \text{and} \quad &z_0 = z, \quad z_1 = \epsilon S x, \quad z_2 = \epsilon^2 S^2 z, \quad \text{etc.,} \end{aligned}\right\} \tag{31}$$

where S is a constant which we shall determine.

According to (31), the multiple-scale expansions of the derivatives $\partial/\partial\tau$ and $\partial/\partial z$ are respectively

$$\left.\begin{aligned} &\partial/\partial\tau = \partial/\partial\tau_0 + \epsilon^2\,\partial/\partial\tau_2 + \ldots \\ \text{and} \quad &\partial/\partial z = \partial/\partial z_0 + \epsilon S\,\partial/\partial z_1 + \epsilon^2 S^2\,\partial/\partial z_2 + \ldots. \end{aligned}\right\} \tag{32}$$

Expanding u, p and h_θ into Fourier series, we now find:

$$\left.\begin{aligned} u_r^{(n)}(x, z, \tau) &= \sum_{l=-\infty}^{l=+\infty} \hat{u}_l^{(n)}(x, z_1, \ldots, \tau_0, \tau_2, \ldots)\, e^{ila_c z_0}, \\ u_\theta^{(n)}(x, z, \tau) &= \sum_{l=-\infty}^{l=+\infty} \hat{v}_l^{(n)}(x, z_1, \ldots, \tau_0, \tau_2, \ldots)\, e^{ila_c z_0}, \\ u_z^{(n)}(x, z, \tau) &= (-i) \sum_{l=-\infty}^{l=+\infty} \hat{w}_l^{(n)}(x, z_1, \ldots, \tau_0, \tau_2, \ldots)\, e^{ila_c z_0}, \\ p^{(n)}(x, z, \tau) &= \sum_{l=-\infty}^{l=+\infty} \hat{p}_l^{(n)}(x, z_1, \ldots, \tau_0, \tau_2, \ldots)\, e^{ila_c z_0}, \\ \text{and} \quad h_\theta^{(n)}(x, z, \tau) &= (-i) \sum_{l=-\infty}^{l=+\infty} \hat{h}_l^{(n)}(x, z_1, \ldots, \tau_0, \tau_2, \ldots)\, e^{ila_c z_0}. \end{aligned}\right\} \tag{33}$$

Since $u_r^{(n)}$, $u_\theta^{(n)}$, $u_z^{(n)}$, $p^{(n)}$ and $h_\theta^{(n)}$ are real, it follows that

$$\hat{u}_l^{(n)} = \hat{u}_l^{(n)*}, \quad \hat{v}_l^{(n)} = \hat{v}_{-l}^{(n)*}, \quad \hat{w}_l^{(n)} = -\hat{w}_{-l}^{(n)*}, \quad \hat{p}_l^{(n)} = \hat{p}_{-l}^{(n)*} \quad \text{and} \quad \hat{h}_l^{(n)} = -\hat{h}_{-l}^{(n)*}$$

for any l and n. To first order, the parameter ϵ reduces to $[(T/T_c)^{\frac{1}{2}} - 1]^{\frac{1}{2}}$ as shown by equation (30).

We now substitute (27)–(33) into the full nonlinear equations of flow (8)–(12) and identify in them each power of ϵ and each Fourier component as introduced above. For $n = 1$ and $l = 1$, we have

$$\left.\begin{aligned} [(D^2 - a_c^2)^2 + Qa_c^2]\, u_1^{(1)} &= T_c^{\frac{1}{2}} a_c u_\theta^{(0)} (D^2 - a_c^2)\, h_1^{(1)} \\ \text{and} \qquad [(D^2 - a_c^2)^2 + Qa_c^2]\, h_1^{(1)} &= T_c^{\frac{1}{2}} a_c D u_\theta^{(0)}\, u_1^{(1)}, \end{aligned}\right\} \tag{34}$$

with

$$u_1^{(1)} = Du_1^{(1)} = (D^2 - a_c^2)\, h_1^{(1)} = 0, \quad \text{and} \quad h_1^{(1)} = 0 \text{ (case I)} \quad \text{or} \quad Dh_1^{(1)} = 0 \text{ (case C)}$$
$$\text{on} \quad x = 0 \quad \text{and} \quad x = 1, \tag{35}$$

where

$$\hat{u}_1^{(1)} = A(z_1, \ldots, \tau_0, \tau_1, \ldots)\, u_1^{(1)} \quad \text{and} \quad \hat{h}_1^{(1)} = A(z_1, \ldots, \tau_0, \tau_1, \ldots)\, h_1^{(1)}.$$

The system of equations (34) together with (35) is equivalent to the characteristic value problem (18) defined in § 2.

Turning to the case $n = 2$, $l = 0$, we find

$$\left.\begin{aligned} u_1^{(1)} Du_1^{(1)} &= -Dp_0^{(2)} - Qu_0^{(2)} + D^2 u_0^{(2)} + T^{\frac{1}{2}} u_\theta^{(0)} v_0^{(2)} + v_1^{(1)2}/2, \\ \tfrac{1}{2} D(u_1^{(1)} v_1^{(1)}) &= D^2 v_0^{(2)} - T^{\frac{1}{2}} u_0^{(2)} Du_\theta^{(0)} \\ \text{and} \qquad D^2 w_0^{(2)} &= D^2 h_0^{(2)} = Du_0^{(2)} = 0, \end{aligned}\right\} \tag{36}$$

together with

$$u_0^{(2)} = v_0^{(2)} = w_0^{(2)} = 0,$$

and

$$h_0^{(2)} = 0 \text{ (case (I))} \quad \text{or} \quad Dh_0^{(2)} = 0 \text{ (case (C))} \quad \text{on} \quad x = 0 \quad \text{and} \quad x = 1,$$

in which we have

$$\hat{u}_0^{(2)} = 4\,|A|^2 u_0^{(2)}, \quad \hat{v}_0^{(2)} = 4\,|A|^2 v_0^{(2)}, \quad \text{etc.}$$

Equations (36) give $u_0^{(2)} = w_0^{(2)} = h_0^{(2)} = 0$, and

$$v_0^{(2)} = \frac{1}{2}\left[\int_0^x u_1^{(1)} v_1^{(1)}\, dx - x \int_0^1 u_1^{(1)} v_1^{(1)} dx\right]. \tag{38}$$

The case $n = 2$, $l = 1$ leads to an equation of the form

$$-2ia_c (\partial A/\partial z_1)(\tilde{\phi}_1 |\, \mathscr{D}_1\, | \phi_1) = 0, \tag{39}$$

where

$$\phi_1^{(1)} = \begin{pmatrix} u_1^{(1)} \\ h_1^{(1)} \end{pmatrix} \quad \text{and} \quad \tilde{\phi}_1^{(1)} = \begin{pmatrix} \tilde{u}_1^{(1)} \\ \tilde{v}_1^{(1)} \end{pmatrix}$$

are the eigenvectors of system (34), (35) and of its adjoint respectively. Owing to the choice of the eigenvalue T_c and the wave number a_c as defined in § 2, the equality (39) is clearly satisfied.

For $n = 2$, $l = 2$, we find

$$\left.\begin{aligned}[(D^2-4a_c^2)^2+4Qa_c^2]\,u_2^{(2)}-2T_c^{\frac{1}{2}}a_c u_\theta^{(0)}(D^2-4a_c^2)\,h_2^{(2)}\\ = D[u_1^{(1)}D^2u_1^{(1)}-(Du_1^{(1)})^2]+[(D^2-a_c^2)\,h_1^{(1)}]^2\\ [(D^2-4a_c^2)^2+4Qa_c^2]\,h_2^{(2)}-2T_c^{\frac{1}{2}}a_c Du_\theta^{(0)}u_2^{(2)}\\ = u_1^{(1)}(D^2-a_c^2)\,Dh_1^{(1)}-Du_1^{(1)}(D^2-a_c^2)\,h_1^{(1)},\end{aligned}\right\} \tag{40}$$

and

together with

$$u_2^{(2)} = Du_2^{(2)} = (D^2-4a_c^2)\,h_2^{(2)} = 0$$

and

$$h_2^{(2)} = 0 \text{ (case (I))} \quad \text{or} \quad Dh_2^{(2)} = 0 \text{ (case C)} \quad \text{on} \quad x = 0,\ 1 \tag{41}$$

where we have $\hat{u}_2^{(2)} = 2A^2u_2^{(2)}$ and $\hat{h}_2^{(2)} = 2A^2h_2^{(2)}$. Now for $n = 3$ and $l = 1$, we find (after some algebra)

$$\begin{aligned}&[(D^2-a_c^2)^2+Qa_c^2]\,\hat{u}_1^{(3)}-T_c^{\frac{1}{2}}a_c u_\theta^{(0)}(D^2-a_c^2)\,\hat{h}_1^{(3)}\\ &\quad = (\partial A/\partial\tau_2-S^2\,\partial^2A/\partial z_1)\,(D^2-a_c^2)\,u_1^{(1)}+Au_\theta^{(0)}a_c(D^2-a_c^2)\,h_1^{(1)}\\ &\qquad -A\,|A|^2\{3a_c^2u_1^{(1)}Du_2^{(2)}+6a_c^2u_2^{(2)}Du_1^{(1)}-2v_1^{(1)}a_c(v_2^{(2)}+2v_0^{(2)})\\ &\qquad -D(u_1^{(1)}D^2u_2^{(2)}-2u_2^{(2)}D^2u_1^{(1)}+Du_1^{(1)}Du_2^{(2)})\},\end{aligned} \tag{42}$$

and

$$\begin{aligned}&[(D^2-a_c^2)^2+Qa^2]\,\hat{h}_1^{(3)}-T_c^{\frac{1}{2}}a_cDu_\theta^{(0)}\hat{u}_1^{(3)}\\ &\quad = (\partial A/\partial\tau_2-S^2\,\partial^2A/\partial z_1^2)\,(D^2-a_c^2)\,h_1^{(1)}+Aa_cDu_\theta^{(0)}u_1^{(1)}\\ &\qquad +A\,|A|^2\,a_c\{4u_1^{(1)}Dv_0^{(2)}+2u_1^{(1)}Dv_2^{(2)}+2u_2^{(2)}Dv_1^{(1)}+4v_2^{(2)}Du_1^{(1)}+v_1^{(1)}Du_2^{(2)}\},\end{aligned} \tag{43}$$

with

$$\hat{u}_1^{(3)} - D\hat{u}_1^{(3)} - (D^2-a_c^2)\,\hat{h}_1^{(3)}$$

and

$$\hat{h}_1^{(3)} = 0 \text{ (case I)} \quad \text{or} \quad D\hat{h}_1^{(3)} = 0 \text{ (case C)} \quad \text{on} \quad x = 0 \quad \text{and} \quad x = 1. \tag{44}$$

Equations (42)–(44) can be rewritten in the following form

$$(\mathscr{A}-T_c^{\frac{1}{2}}\mathscr{B})\,\vec{\phi}_3^{(1)} = (\partial A/\partial\tau_2-S^2\,\partial^2A/\partial z_1^2)\,K\phi_1^{(1)}+A\mathscr{B}\phi_1^{(1)}+A\,|A|^2\psi_1^{(3)}, \tag{45}$$

in which

$$\vec{\phi}_3^{(1)} = \begin{pmatrix}\hat{u}_3^{(1)}\\ \hat{h}_3^{(1)}\end{pmatrix}$$

and $\psi_1^{(3)}$ is defined as

$$\psi_1^{(3)} = \begin{pmatrix}3a_c^2u_1^{(1)}Du_2^{(2)}+6a_c^2u_2^{(2)}Du_1^{(1)}-2v_1^{(1)}a_c(v_1^{(2)}+2v_0^{(2)})\\ -D(u_1^{(1)}D^2u_2^{(2)}-2u_2^{(2)}Du_2^{(1)}+Du_1^{(1)}Du_2^{(2)})\\ 4u_1^{(1)}Dv_0^{(2)}+2u_1^{(1)}Dv_2^{(2)}+2u_2^{(2)}Dv_1^{(1)}+4v_2^{(2)}Du_1^{(1)}+v_1^{(1)}Du_2^{(2)}\end{pmatrix}.$$

The solvability condition applied to (45) leads to the equation

$$(\partial A/\partial\tau_2-S^2\,\partial^2A/\partial z_1^2)\,(\vec{\phi}_1^{(1)}|\,K\,|\phi_1^{(1)})+A(\vec{\phi}_1^{(1)}|\,\mathscr{B}\,|\phi_1^{(1)})+A\,|A|^2\,(\vec{\phi}_1^{(1)}|\,\psi_1^{(3)}) = 0. \tag{46}$$

Now identifying linear terms in (46) with the expansion (43), leaves $S = (c_1/c_0)^{\frac{1}{2}}$ and hence the amplitude equation for the velocity disturbance is found to be (to the relevant order)

$$\frac{\partial A'}{\partial\tau} = \left\{c_0\left[\left(\frac{T}{T_c}\right)^{\frac{1}{2}}-1\right]+c_1\frac{\partial^2}{\partial z^2}\right\}A'-c_2A'\,|A'|^2, \tag{47}$$

where $A' = [(T/T_c)^{\frac{1}{2}} - 1]A$, and where $c_2 = (\tilde{\phi}_1^{(1)}|\psi_1^{(3)})/(\tilde{\phi}_1^{(1)}|\,K\,|\phi_1^{(1)})$ is the amplitude saturation parameter due to nonlinear effects.

The stationary equilibrium amplitude of the disturbances is governed by the equation

$$\xi_0^2\,\partial^2 A^1/\partial z^2 = -\epsilon A' + A'^3/A_0'^2 \tag{48}$$

with

$$A_0' = (c_2/c_0)^{\frac{1}{2}} \quad \text{and} \quad \xi_0 = (c_1/c_0)^{\frac{1}{2}}. \tag{49}$$

Equation (48) defines A as a function of the distance z and a reduced penetration length $\xi = \xi_0(2/\epsilon)^{\frac{1}{2}}$. On physical grounds, equation (48) means that the amplitude of the Taylor vortices is slightly modulated throughout the annular space, on account of end-wall effects. In the case when the aspect ratio L/d is large (i.e. $L/d \gg \xi$, where L is the cylinder length), $A(z, \xi)$ is virtually constant in the major part of the duct, and decreases to zero in small boundary layers near the end walls. Such regions have $O(\xi)$ as characteristic length scale. In such conditions, the mean spatial properties of the flow (such as the velocity flux) are approximately the same as in the infinite case.

It is clear that equation (48) gives an incomplete description of finite-cylinder effects on the flow above transition. Realistic description of such effects requires careful statement of the linear stability problem: see Blennerhasset & Hall (1979) or others for studies on the subject in absence of magnetic field.

Now we are in position to calculate stationary spatially average quantities, such as the torque G exerted along the inner cylinder and the mean velocity U_m calculated throughout the annular space. Assuming that we have $d/L \sim 0$ we find:

$$G = 2\pi R_1^2 L\tilde{\eta} \int_{-L/2}^{L/2} (\partial U_\theta/\partial X)_{X=0}\,dZ = 2\pi R_1 L U_e \rho\nu/d^{-1}(Du_\theta^{(0)})_{X=0}\{1 + \gamma[1 - (T_c/T)^{\frac{1}{2}}]\}, \tag{50}$$

and

$$U_m = \frac{1}{Ld}\int_0^d \int_{-L/2}^{L/2} U_\theta(x, z)\,dx\,dz = U_e\langle u_\theta^{(0)}\rangle\{1 + \kappa[1 - (T_c/T)^{\frac{1}{2}}]\}, \tag{51}$$

in which

$$\gamma = (c_0/c_2)\,T_c^{-\frac{1}{2}}(Dv_0^{(2)})_{x=0}/(Du_\theta^{(0)})_{x=0}, \tag{52}$$

and

$$\kappa = (c_0/c_2)\,T_c^{-\frac{1}{2}}\langle v_0^{(2)}\rangle/\langle u_\theta^{(0)}\rangle. \tag{53}$$

5. Numerical method of solution

The numerical method of solution used for determining eigenvalues and eigenvectors of (18) has been described in a previous paper (Tabeling & Chabrerie 1981*a*). The method consists in rewriting (18) as a first-order differential system including eight functions, and solving this by the Runge–Kutta–Gill method.

Eigenvalues T_j are then calculated in such a way that solutions of (18), obtained for a given set of boundary conditions, are linearly dependent. Further, the critical Taylor number T_c and critical wavenumber are simply calculated as those values of T_1 and a defining a minimum point on the neutral curves. Once the critical point is found, the adjoint system (20) and the equations (40), (41) are solved by means of the Runge–Kutta–Gill technique, the various integrals involved in the problem being calculated by simple trapezium rules. The resulting accuracy on a_c and T_c is 10^{-2} and 10^{-4} respectively, and that on c_0, c_1 and c_2 is better than 4×10^{-2}.

6. Numerical results

6.1. *Taylor–Couette flows between insulating cylinders*

In the case of Taylor–Couette flow without a transverse pressure gradient, the velocity scale U_c is simply $\Omega_1 R_1$ and hence the Taylor number is defined (see (13)) by

$$T = (\Omega_1 R_1 d/\nu)^2 d/R_1.$$

Hereafter we present calculations on Taylor–Couette flows between insulating cylinders, in the range $0 \leqslant Q \leqslant 10^6$. Results on the critical point (T_c, a_c) are found to be in excellent agreement with previous numerical studies (Chandrasekhar 1961), over the entire range of values of Q considered. Asymptotic laws obtained at large values of Q are

$$a_c = 15{\cdot}1Q^{-\frac{1}{2}} \quad \text{and} \quad T_c = 107{\cdot}2Q,$$

which shows that Taylor cells tend to elongate along magnetic field lines when Q is increased.

Coefficients c_0 and ξ_0. Figure 2 shows the coefficients c_0 and $\xi_0 = (c_1/c_0)^{\frac{1}{2}}$ versus Q, calculated from equations (24) and (25). At $Q = 0$, results on c_0 and ξ_0 are in excellent agreement with calculations of Davey (1962), and Yahata (1977), performed on the same flow without the magnetic field. Curves in figure 2 show that both c_0 and ξ_0 increase when Q is increased, although in different ways. Asymptotic laws deduced from the present study are

$$c_0 \to 43{\cdot}2 \quad \text{and} \quad \xi_0 \sim 4{\cdot}1Q^{\frac{1}{2}},$$

when Q tends to infinity. Asymptotic behaviours as found above can also be deduced from order-of-magnitude arguments. On physical grounds, the present results show that

(i) the characteristic time scale of the marginal state is, for a given discrepancy $\epsilon^2 = (T/T_c)^{\frac{1}{2}} - 1$, the viscous time d^2/ν;

(ii) finite-length effects penetrate the flow through a distance of a few cells, multiplied by a factor $(2/\epsilon)^{\frac{1}{4}}$.

Effect (i) is clearly explained by the fact that, at the onset of instability, Joule and viscous dissipations have the same order of magnitude and, hence, involve a single characteristic time scale, i.e. d^2/ν for the marginal state.

Disturbance velocity profiles. Velocity profiles $\hat{v}_2^{(2)} T_c^{-\frac{1}{2}}$ calculated for $Q = 0$, 10^4, and with $d/L = 0$, are shown in figure 3. Curve (a) obtained when $Q = 0$ is in excellent agreement with results of Davey (1962). When Q is increased, the level of the first harmonic of the velocity disturbance slowly increases: however, numerical results indicate that the harmonic remains small in comparison with the fundamental and hence no dramatic increase in the harmonic content of the flow, due to the magnetic field, occurs in this case.

Torque exerted along the inner cylinder. Using formula (50) we find:

$$G = 2\pi R_1^3 \Omega_1 L \tilde{\eta}/d^{-1}\{1 + \gamma[1 - (T_c/T)^{\frac{1}{2}}]\}, \tag{55}$$

where

$$\gamma = \frac{2c_0}{c_2} T_c^{-\frac{1}{2}} \int_0^1 u_1^{(1)} v_1^{(1)}\, dx. \tag{56}$$

Figure 4 represents the curve $\gamma(Q)$; it turns out that the magnetic field tends to reduce, by a small amount, the relative increase in the torque due to the cellular motion. At

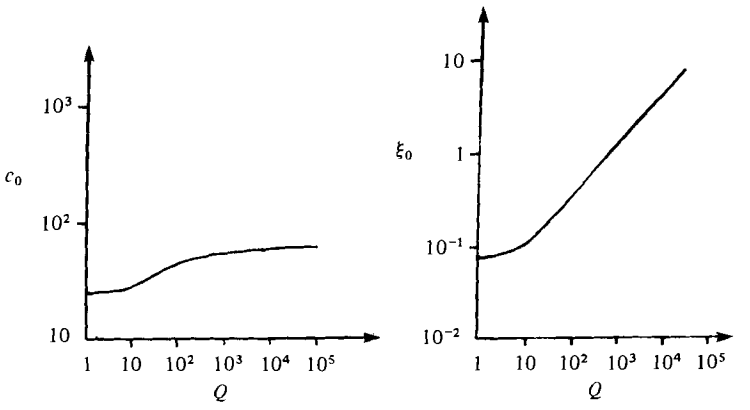

FIGURE 2. Graphs of c_0 and ξ_0 against the Chandrasekhar number Q in Taylor–Couette flow case and when cylinders are insulating.

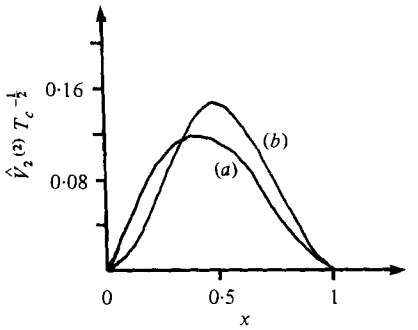

FIGURE 3. Profiles of the first harmonic of the transverse velocity disturbance for (*a*) $Q = 0$, (*b*) $Q = 10^4$.

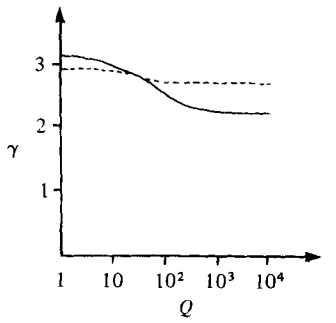

FIGURE 4. Torque coefficient γ versus Q.

$Q = 0$, we find $\gamma = 3{\cdot}05$ (which is in excellent agreement with Davey's results) and, when Q becomes increasingly large, we find that $\gamma \to 2{\cdot}3$.

Also shown in figure 4 is the torque coefficient calculated by Stuart's energizing method (Tabeling & Marsan 1980). Results obtained by the two methods appear to be rather close together, since the discrepancy between them is at most 12 %. Such a feature is due to the fact that, in the case of Taylor–Couette flow between insulating cylinders, the governing operator for linearized stability is nearly self-adjoint (as shown by Chandrasekhar 1961) and the harmonic content of the flow remains small (as pointed out in § 6).

6.2. *Pure pressure-driven flow between conducting steady cylinders*

In the case of pure pressure-driven flow between steady cylinders, we impose $U_e = Kd^2/2\tilde{\eta}$ as the velocity scale, and therefore the Taylor number T and dimensionless laminar primary flow $u_\theta^{(0)}(x)$ are respectively

$$T = 2(K\rho d^3/2\tilde{\eta}^3)^2 d/R_1 \quad \text{and} \quad u_\theta^{(0)}(x) = x(1-x).$$

Further we shall restrict ourselves to the case of flows between perfectly conducting cylinders.

Linearized stability of the flow. The characteristic-value problem (18) has been solved in the range $0 \leqslant Q \leqslant 1100$. Resulting neutral curves obtained for various values of Q are shown in figure 5. At $Q = 0$, the critical value of the Taylor number is found to be in excellent agreement with that calculated by Di Prima (1964). At moderate values of Q, the two lowest branches of the neutral curves consist in a single loop which rises up and recedes to the right of the figure as Q is further increased. In contrast with the preceding flow (Taylor–Couette flow between insulating cylinders) the critical wavenumber increases with Q and hence Taylor cells contract along magnetic field lines when the magnetic field is increased. On physical grounds, this feature has been fairly justified by Chang & Sartory (1967), who showed that, when cylinders are conducting, elongation of the cells does not tend to minimize Joule dissipations. Higher-order modes have not been calculated in detail. However, it turns out that the corresponding neutral curves generally lie above those related to the first two modes. Note that this result means that, if it were possible, in an experiment, to control the wavenumber, one could reach purely laminar states of flow with $T > T_c$.

It is possible to argue from equations (18) that reasonable estimates for a_c and T_c are given by $a_c = O(Q^{\frac{1}{2}})$ and $T_c = O(Q^{\frac{5}{2}})$ when Q is large (see Tabeling 1980) and the reduced characteristic length scale for the marginal state of flow is $O(\tilde{\eta}^{\frac{1}{2}}/\sigma^{\frac{1}{2}}B_0)$ and not $O(d)$.

Coefficients c_0 and ξ_0. Coefficients c_0 and ξ_0 are represented by curves of figure 6. In contrast with previous results on Taylor–Couette flows between insulating cylinders, c_0 significantly increases with Q; numerical estimates indicate that c_0 is roughly proportional to Q over the range $300 \leqslant Q \leqslant 1100$. According to this, the characteristic time-scale for the marginal state of flow is $[(T/T_c)^{\frac{1}{2}} - 1]\rho/\sigma B_0^2$ when Q is large, and not $[(T/T_c)^{\frac{1}{2}} - 1]d^2/\nu$. Physically, such a feature should be viewed as a damping effect of disturbances by the magnetic field.

In figure 6, the curve for ξ_0 decreases when Q is increased. Such a decrease is clearly related with the contraction of Taylor cells along magnetic field lines when Q is increased, as mentioned above. Still in this case, end effects penetrate the flow over a distance of a few cells, multiplied by a factor $(2/\epsilon)^{\frac{1}{2}}$.

The fundamental and the first harmonic of disturbances. Figure 7 shows for various values of Q the fundamental $\hat{v}_1^{(1)} T_c^{-\frac{1}{2}}$ and the first harmonic $\hat{v}_2^{(2)} T_c^{-\frac{1}{2}}$ of the transverse velocity perturbation. When Q is increased, velocity profiles recede to the right of the figure. Although the level of the first harmonic $\hat{v}_2^{(2)} T_c^{-\frac{1}{2}}$ decreases with Q, present calculations indicate that the shear stress $D\hat{v}_2^{(2)}$. $T_c^{-\frac{1}{2}}$ significantly increases with Q near the outer wall $x = 1$. Following Davey (1962), we can separate the saturation coefficient c_2 into two parts (see (45))

$$c_2 = c_{201} + c_{22},$$

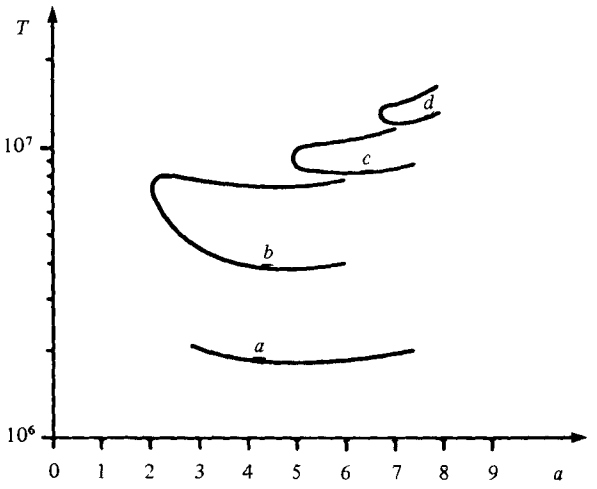

FIGURE 5. Neutral curves for pressure-driven flows between steady conducting cylinders, for various values of Q. (*a*) $Q = 100$; (*b*) $Q = 500$; (*c*) $Q = 800$; (*d*) $Q = 1000$.

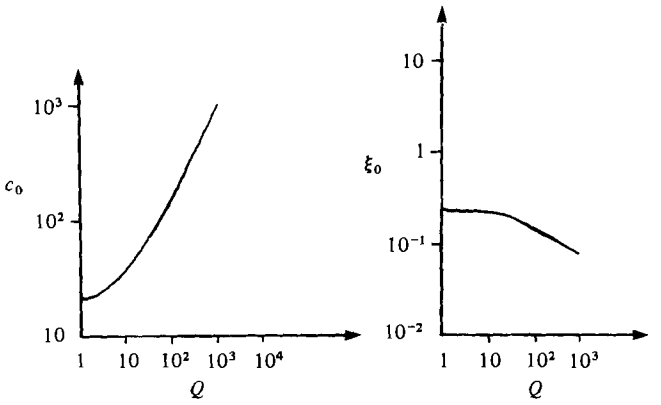

FIGURE 6. Graphs of c_0 and ξ_0 against the Chandrasekhar number Q in the case of pure pressure-driven flows between conducting cylinders.

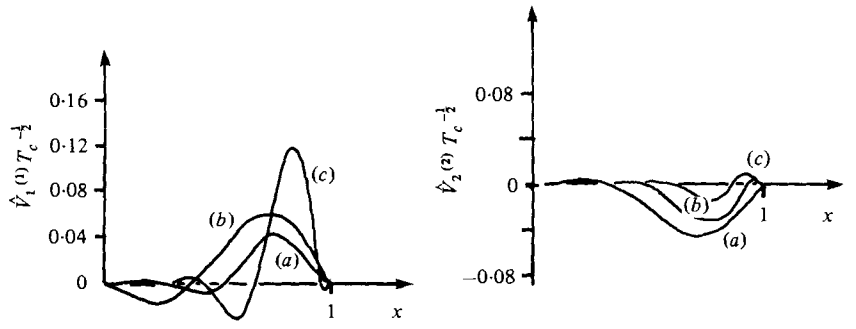

FIGURE 7. Profiles of the fundamental and the first harmonic of the transverse velocity disturbance for various values of Q. (*a*) $Q = 0$; (*b*) $Q = 300$; (*c*) $Q = 1000$.

Q	c_{22}/c_{201}
0	−0·04
100	−0·10
300	−0·25
500	−0·43
700	−0·52
1000	−0·49

TABLE 1

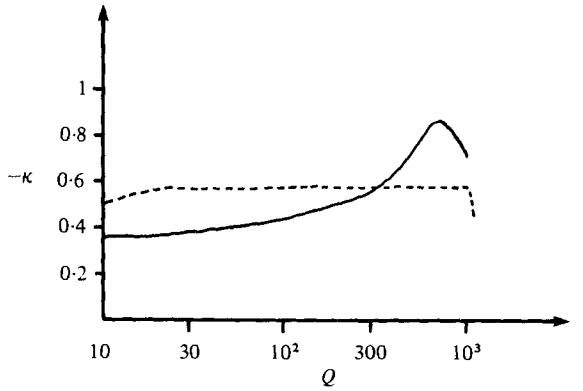

FIGURE 8. Curve of the mean velocity coefficient κ as a function of Q in the case of pure pressure-driven flow between conducting cylinders and calculated by two methods. Solid line, perturbative method; dashed line, Stuart energizing method.

in which

$$c_{201} = \langle -4a_c v_1^{(1)} v_0^{(2)} \tilde{u}_1^{(1)} + 4u_1^{(1)} Dv_0^{(2)} \tilde{h}_1^{(1)} \rangle$$

and

$$\begin{aligned} c_{22} = \langle & \tilde{u}_1^{(1)} [3a_c^2 u_1^{(1)} Du_2^{(2)} + 6a_c^2 u_2^{(2)} Du_1^{(1)} - 2a_c v_1^{(1)} v_2^{(2)}] \\ & - D(u_1^{(1)} D^2 u_2^{(2)} - 2u_2^{(2)} D^2 u_1^{(1)} + Du_1^{(1)} Du_2^{(2)})] \\ & + \tilde{h}_1^{(1)} [2u_1^{(1)} Dv_2^{(2)} + 2u_2^{(2)} Dv_1^{(1)} + 4v_2^{(2)} Du_1^{(1)} + v_1^{(1)} Du_2^{(2)}] \rangle. \end{aligned}$$

c_{201} and c_{22} represent the distortion of the mean motion and the generation of the harmonic respectively. The present calculations show that c_{20} is positive over the entire range of values of Q considered, so that we find that energy is extracted from the mean flow to the fundamental. Now c_{22} is found to be negative so that the harmonic supplies energy to the fundamental. Values of the ratio c_{22}/c_{201} are listed in table 1; c_{22}/c_{201} first increases with Q in the range $0 < Q < 700$, and then slowly decreases. Its maximum value $-0{\cdot}52$ is considerably larger than its value at $Q = 0$, i.e. in absence of the magnetic field. On physical grounds, this means that the magnetic field dramatically reinforces the harmonic content of the flow above transition. Such a feature contrasts with that found in Taylor–Couette flows between insulating cylinders, in which the harmonic has little effect on the flow in the supercritical state. Further calculations, performed in case of pressure-driven flows between insulating cylinders, exhibit a similar increase in the harmonic content of the flow when Q is increased, so that this effect is not strictly related to cylinders' conductivity.

The mean velocity of the flow. Returning to formulas (51) and (53), we find

$$U_m = \frac{1}{Ld}\int_0^1 \int_{-L/2}^{L/2} U_\theta(x,z)\,dx\,dz = \frac{Kd^2}{12\tilde{\eta}}\left\{1+\kappa\left(1-\left(\frac{T_c}{T}\right)^{\frac{1}{2}}\right)\right\}, \tag{58}$$

with

$$\kappa = 6\frac{c_0}{c_2}T_c^{-\frac{1}{2}}\left[\int_0^1\left(\int_0^x uv\,dx\right)-\frac{1}{2}\int_0^1 uv\,dx\right]. \tag{59}$$

Figure 8 represents the function $-\kappa(Q)$, which is found to be everywhere positive; $\kappa(Q)$ first increases (in absolute value) in the range $0 < Q < 700$ and further decreases. A mean velocity coefficient (similar to κ) had been previously calculated by means of Stuart's energy approach (Tabeling & Chabrerie 1981*a*); the latter is also represented in figure 8. It turns out that the discrepancy between the two curves is significant; such a disagreement between the two methods is clearly due to the fact that, in the case of pure pressure-driven flow, the harmonic content is significant and the governing operator for linear stability problem cannot be approximated by a self-adjoint operator; it follows that, in this case, Stuart's energizing approach is imprecise.

7. Comparison with experiment

7.1. *Taylor–Couette flow between insulating cylinders*

Donnelly & Ozima (1962) have performed experiments on Taylor–Couette flows of mercury between two long Perspex cylinders, the inner one rotating and the outer one stationary. The dimensions of their apparatus were

$$R_1 = 1{\cdot}9\,\text{cm}, \quad R_2 = 2{\cdot}0\,\text{cm} \quad \text{and} \quad L = 10\,\text{cm},$$

so that the curvature ratio $\delta = d/R_1$ is small. Figure 8 shows experimental results on the ratio

$$\tilde{\eta}^*/\tilde{\eta}_c^* = G/2\pi R_1 L\Omega_1\tilde{\eta}_c^*, \tag{60}$$

as a function of the angular speed Ω_1 for given values of Q. In (60), η_c^* is the experimental critical value.for the effective viscosity $\tilde{\eta}^*$. Due to Hartmann end effects, the latter is slightly larger than the mercury viscosity. Using (54)–(56) and (60) then gives for $\tilde{\eta}^*/\tilde{\eta}_c^*$ an expression of the form

$$\tilde{\eta}^*/\tilde{\eta}_c^* = 1+\gamma(1-\Omega_{1c}/\Omega_1), \tag{61}$$

in which Ω_{1c} is the critical value of Ω_1 at the onset of instability. Theoretical curves (61) are represented by solid lines in figure 9. At $Q = 0$, experimental points leave the theoretical curve slightly above transition. This corresponds to the onset of wavy vortices, as shown by Stuart (1971) or others. When Q is increased, good agreement is found between theory and experiment over an increasing range of values of Ω_1. Departures of experimental points from the solid lines probably correspond to further instabilities; in any event the onset of wavy vortices clearly appears to be significantly inhibited by the magnetic field. Thus, in the present flow, theory and experiment are found to be in good agreement over the range of values of Ω_1 for which we expect the method to be valid.

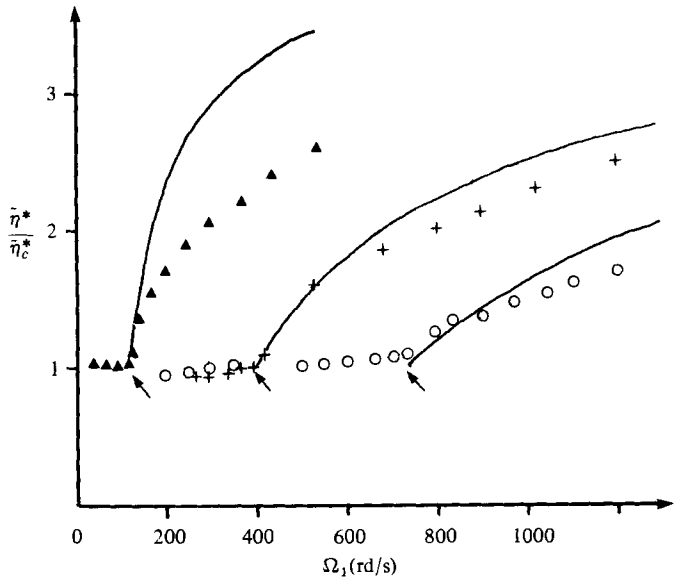

FIGURE 9. Comparison between theory (solid line) and experiments in the case of Taylor–Couette flow between insulating cylinders. ▲, $Q = 0$; +, $Q = 180$; ○, $Q = 652$.

7.2. *Pressure-driven flows between conducting cylinders*

Tabeling & Chabrerie (1981*b*) have performed experiments on electromagnetically driven flows of mercury between two long steady copper cylinders in the range $20 \leqslant Q \leqslant 1083$. In their experiments, the total electromagnetic driving force $B_0 Id$ (where I is the current flowing from one cylinder to the other) gives rise to a constant transverse body force

$$K = B_0 Id/2\pi R_1 L,$$

as defined in § 2. The dimensions of the apparatus are

first group:	$R_1 = 4{\cdot}0$ cm;	$R_2 = 4{\cdot}05$ cm;	$L = 3{\cdot}94$ cm;
second group:	$R_1 = 3{\cdot}9075$ cm;	$R_2 = 3{\cdot}9475$ cm;	$L = 1{\cdot}3$ cm.

Figure 2 shows the ratio

$$\tilde{\eta}^*/\tilde{\eta}_c^* = B_0 Id^2/4\pi R_1 L \tilde{\eta}_c^* U_m, \tag{62}$$

as a function of the total driving force $B_0 Id$, for various values of Q. In (62), $\tilde{\eta}_c^*$ is the critical value for the effective viscosity $\tilde{\eta}^* = B_0 Id^2/4\pi R_1 L U_m$. As in the preceding section, experimental values of $\tilde{\eta}_c^*$ are slightly greater than the mercury viscosity; this is essentially due to Hartmann end effects. In the present experiments, critical points of instability are found to be in good agreement with results of linearized stability theory for axisymmetric stationary disturbances over the range $0 < Q < 1100$.

Now turning to the supercritical state of flow, and noting that d/L is very small in these experiments, we use (57)–(59) and (62) to find

$$\tilde{\eta}^*/\eta_c^* = [1 - \kappa(1 - I_c/I)]^{-1}, \tag{63}$$

where I_c is the critical value for the driving current I at transition. Expressions (63) are represented by solid lines in figure 10. Also represented in figure 10(*a*) is the

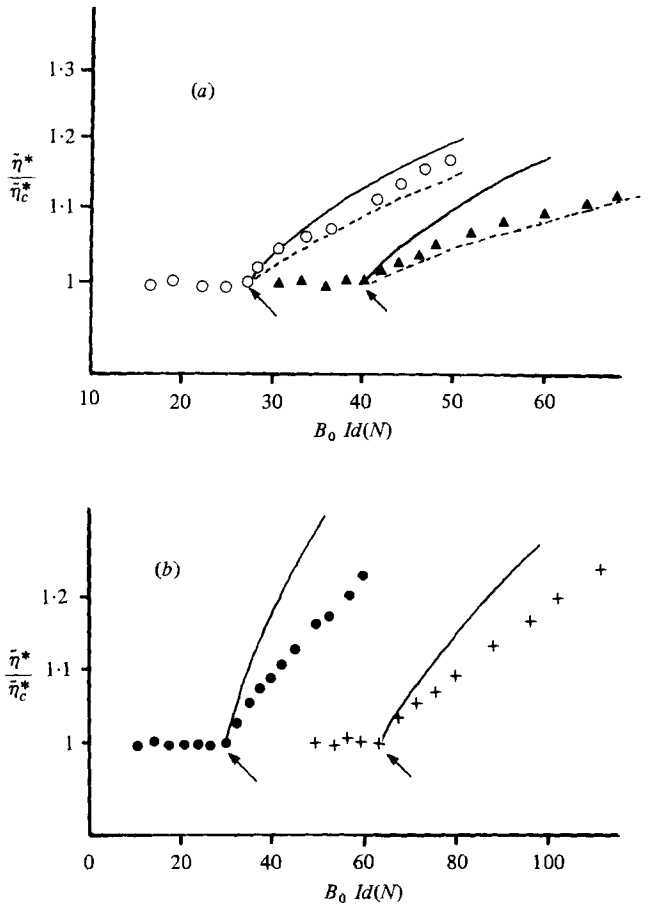

FIGURE 10. Comparison between theory (solid line) and experiments in case of pure pressure-driven flows between conducting cylinders. ○, $Q = 45$; ▲, $Q = 107$; ●, $Q = 376$; +, $Q = 1085$. Results deduced from Baylis's experiments are shown by dashed lines.

empirical law deduced from Baylis's experiments, and given by

$$\tilde{\eta}^*/\tilde{\eta}_c^* = (I/I_c)^{0\cdot20}$$

over the range $0 < Q < 160$. Experimental data of Tabeling & Chabrerie and Baylis are found to be close together as shown in figure 10(*a*). It turns out that theory and experiment are in moderate agreement for $Q = 45$, while in significant disagreement at larger values of Q. This result contrasts with that obtained for the preceding flow, in which experimental points are well fitted by theoretical curves over a large range of values of Q (see § 7.1). The present discrepancy between theory and experiment is partly due to the fact that, even at moderate values of Q, the harmonic content of the flow is significant (as shown in § 6), so that the perturbation method loses accuracy in the corresponding range of values of Q, once $(T/T_c)^{\frac{1}{2}} - 1$ ceases to be very small. There are other possible reasons for the discrepancy: Volkov *et al.* (1976) indicate that, for $Q > 625$, non-axisymmetric oscillatory modes are slightly more critical than stationary ones; also of importance is the onset of further instabilities, just above transition: since significant distortion of the mean stream tends to develop only in thin regions

near the outer cylinder (even at moderate values of Q, as shown in § 6) the stationary cellular flow may be expected to be unstable. Now, other types of supercritical instabilities may be mentioned such as those emanating from the structure of the flow itself, with regard to the large number of cells included in the system (from 40 to 60 cells in Tabeling and Chabrerie's experiment).

8. Conclusion

The present study shows that nonlinear stability theory can be successfully extended to a more general class of flows, such as those subjected to an external magnetic field. In the case of Taylor–Couette flows between insulating cylinders, the good agreement between theory and experiment strongly suggests that the onset of wavy vortices is delayed by the magnetic field. One can conjecture that the sequences of instabilities leading to turbulence is also affected by the external magnetic field. In the case of electromagnetically driven flows, the situation appears to be more complex. Recent measurements suggest that overstability plays an important role once magnetic field effects become significant. However, additional information on the subject is clearly required.

REFERENCES

Baylis, J. A. 1962 Ph.D. Dissertation, Cambridge University.

Blennerhasset, P. & Hall, P. 1979 *Proc. Roy. Soc.* A **365**, 191.

Chandrasekhar, S. 1961 *Hydrodynamic and Hydromagnetic Stability*, pp. 382–425. Oxford University Press.

Chang, T. S. & Sartory, W. K. 1967 *Proc. Roy. Soc.* A **301**, 541.

Davey, A. 1962 *J. Fluid Mech.* **14**, 336.

DiPrima, R. C. 1964 *ASLE Trans.* **7**, 333.

Donnelly, R. J. & Ozima, M. 1962 *Proc. Roy. Soc.* A **266**, 272.

Moffatt, H. K. 1962 Ph.D. Dissertation, Cambridge University.

Stuart, J. T. 1971 *Ann. Rev. Fluid Mech.* **3**, 347.

Tabeling, P. & Chabrerie, J. P. 1981*a* *Phys. Fluids* **29**, 406.

Tabeling, P. & Chabrerie, J. P. 1981*b* *J. Fluid Mech.* **103**, 225.

Tabeling, P. 1980 Thèse Université, Paris VI.

Tabeling, P. & Marsan, I. 1980 *Phys. Lett.* A **75**, 217.

Volkov, A. V., Gurfink, M. M. & Poluektov, A. P. 1976 *Magnetohydrodynamika* **1**, 81.

Yahata, H. 1977 *Prog. Theor. Physics* **57**, 347.